

Article

Gas Sensing Studies of an n-n Hetero-Junction Array Based on SnO₂ and ZnO Composites

Anupriya Naik ¹, Ivan Parkin ¹ and Russell Binions ^{2,*}

¹ Christopher Ingold Laboratories, Department of Chemistry, University College London, 20 Gordon Street, London, WC1H 0AJ, UK; a.naik@ucl.ac.uk (A.N.); i.p.parkin@ucl.ac.uk (I.P.)

² School of Engineering and Materials Science, Queen Mary University of London, Mile End Road, London, E1 4NS, UK

* Correspondence: r.binions@qmul.ac.uk; Tel.: +44-20-7882-5305

Academic Editor: Igor Medintz

Received: 23 November 2015; Accepted: 26 January 2016; Published: 4 February 2016

Abstract: A composite metal oxide semiconductor (MOS) sensor array based on tin dioxide (SnO₂) and zinc oxide (ZnO) has been fabricated using a straight forward mechanical mixing method. The array was characterized using X-ray photoelectron spectroscopy, scanning electron microscopy, Raman spectroscopy and X-ray diffraction. The array was evaluated against a number of environmentally important reducing and oxidizing gases across a range of operating temperatures (300–500 °C). The highest response achieved was against 100 ppm ethanol by the 50 wt% ZnO–50 wt% SnO₂ device, which exhibited a response of 109.1, a 4.5-fold increase with respect to the pure SnO₂ counterpart (which displayed a response of 24.4) and a 12.3-fold enhancement with respect to the pure ZnO counterpart (which was associated with a response of 8.9), towards the same concentration of the analyte. Cross sensitivity studies were also carried out against a variety of reducing gases at an operating temperature of 300 °C. The sensors array showed selectivity towards ethanol. The enhanced behaviour of the mixed oxide materials was influenced by junction effects, composition, the packing structure and the device microstructure. The results show that it is possible to tune the sensitivity and selectivity of a composite sensor, through a simple change in the composition of the composite.

Keywords: environmental gas sensing; hetero-junctions; metal oxide sensors; SnO₂; ZnO

1. Introduction

The use of mixtures of semiconducting metal oxide gas-sensitive materials based on semiconducting metal oxides is a relatively recent field of research within chemical sensors [1]. Such research is inspired by the fact that these materials display various desirable traits, such as improved sensitivity, enhanced adsorption ability, extensive catalytic activity, and high thermodynamic stability; however, finding all of these benefits in a single oxide material has proved to be difficult [2]. The use of metal oxide composites or mixtures of metal oxides can however, lead to novel materials that display many of these highly desirable properties [1,3–8].

The use of such composite material systems in gas sensing has been reported in a number of papers in the literature [2,7,9–12], suggesting that enhanced gas response behaviour is promoted as a result of synergistic effects between the two different composite components. Zakrzewska [12] pursued a theoretical approach and reported that the formation of such composite oxides modifies the system's electronic structure through changes in its associated bulk and surface components. The surface component of such systems is affected in all types of composite oxide systems, and new grain boundaries that are formed between different materials are expected to be highly directing regards the

gas sensing properties of the system [12]. Indeed, it has been reported that it is such grain boundaries between the different semiconducting oxide materials of the composites, or the hetero-junctions, that are the main driver of the enhancement effects observed in many composite gas sensor systems [13–16].

In the work reported in this paper, we investigate isotype hetero-junctions [17], as both materials of the composite are n-type semiconducting oxides. When two solids that have different work functions are brought into contact, then the Fermi level must come to be in an electrostatic equilibrium [18]. This equilibrium state is reached because the electrons from the component with the lower work function flow to the higher work function component until such an equilibrium is established [19]. The concept of Fermi level equilibration has been widely reported from a number of different papers [17,18]. For example, Zeng *et al.* [20] recently reported the enhanced gas sensing properties of TiO₂ nanobelts functionalized with SnO₂ nanospheres towards a variety of gases including formaldehyde, ethanol, methanol, and acetone. They report that the contact regions between both semiconducting oxide components plays a fundamental role in inducing more active gas reactions and increased gas sensitivity of the system. Yamazoe *et al.* [18,21] complemented this work introducing the concept of contact potential, $q\delta_p$, defined in Equation (1) [18,21]:

$$q\delta_p = (E_{F2(f)} - E_{F1(f)}) = q\phi_{1(f)} - q\phi_{2(f)} \quad (1)$$

where $q\Phi_{1(f)}$ and $q\Phi_{2(f)}$ or $E_{F1(f)}$ and $E_{F2(f)}$ are work function or conduction band energies of Grain 1 and Grain 2 at the free state, respectively. They suggest that this potential is always generated in the presence of a hetero-contact or actually where a contact between grains where non-uniformity exists either sides of the junction. This electrostatic equilibrium causes a difference in the conduction band edge (δ_{EC}), between the contacting grains that allows for an exchange of the flow of current across the contact. Yamazoe *et al.* have further shown that this contact potential acts to attenuate the drift mobility, μ , of electrons that travel in the direction against it. As such it influences the resistance (increasing the resistance) of the associated contact [18,21]. The electrical properties of the contact are thus sensitive to the local environment in two distinct ways: first of all, through a change in the electron density at the surface of the grains and secondly through a change in the drift mobility of the electron flow. It has been suggested that such hetero-contact resistance is more sensitive than homo-contact resistance. Therefore, exploitation of hetero-contact systems ought to lead to a new generation of highly gas responsive devices [18,21].

In this paper, we report a study on the gas sensing properties of an isotype hetero-junction gas sensor array based on composite mixtures of SnO₂ and ZnO. We discuss the influence of various chemical and physical properties, such as sensor operating temperature, analyte gas concentration, sensor device composition and microstructure, as well as inferring hetero-junction and packing structure effects on the gas response characteristics.

2. Experimental Section

An array of SnO₂ and ZnO (both Sigma Aldrich), pure and mixed-oxide MOS sensors was fabricated as shown in Table 1. This involved mixing various quantities of each component metal oxide powder. Inks of the pure and mixed-oxide materials were subsequently prepared via mechanical mixing of the powders in an organic vehicle - ESL 400 (Agmet. Ltd) in an agate pestle and mortar. The inks were then screen-printed using a DEK 1202 screen-printer onto individual strips of gas sensor substrates. Gas sensor substrates (Capteur Sensors) were 2 mm × 2 mm wide-gap alumina chips with inter-digitated gold electrodes, with an electrode gap of ~155 μm between the electrodes. 4 layers of each ink were screen-printed (each separate print was dried under an infra-red lamp for 10 min, before printing the next layer) onto individual strips. The strips were fired in a furnace (Elite Thermal Systems Limited) at 600 °C for 1 h, to burn off the organic vehicle. Spot welding was then performed on each individual chip, which required platinum wires (50.8-μm in diameter, 99.95% metal basis, Alfa Aesar) to be spot welded to the platinum heater track at the bottom and the gold electrodes on the top

of the gas sensor chips, using a Macgregor DC601 parallel gap resistance welder. The chips were then further welded onto individual sensor device housings.

Table 1. MOS sensor devices fabricated for this work. Those sensor devices with an asterisk (*) are single-component metal oxide MOS sensor devices; all others are dual component metal oxide MOS sensor devices.

Sensor Device	Metal Oxide Powder(s) and Mass (g)	Metal Oxide Powder(s) and Moles (mol)	Mass of ESL 400 (g)
*100 wt% SnO ₂	SnO ₂ –2.10	SnO ₂ –0.014	1.61
90 wt% SnO ₂ – 10 wt% ZnO	SnO ₂ –1.83 ZnO–0.21	SnO ₂ –0.012 ZnO–0.003	1.24
70 wt% SnO ₂ – 30 wt% ZnO	SnO ₂ –1.42 ZnO–0.62	SnO ₂ –0.009 ZnO–0.008	0.74
50 wt% SnO ₂ – 50 wt% ZnO	SnO ₂ –1.51 ZnO–1.52	SnO ₂ –0.010 ZnO–0.019	1.08
30 wt% SnO ₂ – 70 wt% ZnO	SnO ₂ –0.60 ZnO–1.41	SnO ₂ –0.004 ZnO–0.017	0.85
10 wt% SnO ₂ – 90 wt% ZnO	SnO ₂ –0.21 ZnO–1.80	SnO ₂ –0.001 ZnO–0.022	1.06
*100 wt% ZnO	ZnO–2.00	ZnO–0.025	1.18

2.1. Materials Characterisation

Scanning electron microscopy (SEM) images were acquired using a Jeol JSM-6301F field emission scanning microscope. X-ray diffraction (XRD) was carried out on the sensor chips using a micro focus Bruker Discover D8 diffractometer with a wide angle Gadds detector utilising Cu K α_{1+2} radiation ($\lambda = 1.546 \text{ \AA}$) in reflection mode with an incident angle of 5° . Raman spectroscopy was carried out using a Renishaw inVia Raman (Renishaw Raman System 1000) microscope using an argon-ion laser with a wavelength of 514.5 nm. X-ray photoelectron spectroscopy (XPS) was carried out with a Thermo K-Alpha spectrometer utilising monochromated Al K α radiation. Survey scans were collected over the 0–1400 eV binding energy range with a 1 eV step size and a pass energy of 200 eV. Higher resolution scans (0.1 eV step size) were carried out around the principle peaks for each element and were collected at a pass energy of 50 eV.

2.2. Gas Sensing Characterisation

Gas sensing experiments were carried out using an automated test rig that was designed and built at UCL that has been reported previously [22]. The sensors were held at constant operating temperatures via a Whetstone bridge circuit connected to each sensors' platinum heater track. The heater circuits were used to set the sensors at a range of operating temperatures between 300 °C and 500 °C, in 50 °C increments. Sensor conductance and resistance measurements were obtained using potentiostat circuits and tested against a range of environmentally important gases: NO₂ (100–800 ppb), ethanol (5–100 ppm), acetone (1–10 ppm), CO (100–1000 ppm) and NH₃ (5–20 ppm). In all cases the dilution gas was compressed air. All gases were obtained from the British Oxygen Company and used without further treatment. Gas response was defined as either R/R_0 (resistive response) or R_0/R (conductive response), where R_0 is the sensor baseline resistance in air and R is the sensor resistance when exposed to test gas.

3. Results and Discussion

3.1. Scanning Electron Microscopy

SEM imaging characterisation of all seven sensors in the SnO₂-ZnO composite array was carried out to gauge the microstructure of each material.

SEM imaging of the sensor devices showed that the ZnO sample observed in Figure 1a,b consisted of three-dimensional cuboid-shaped particles with curved edges, with a broad particle size distribution ranging between 0.1 and 1 μm . The morphology of the SnO₂ material observed in Figure 1m,n was attributed to smooth and jagged rock-like clumps ranging from a size of 0.25 μm to as large as 1.75 μm . The image of the 10 wt% ZnO–90 wt% SnO₂ in Figure 1l showed that some of the SnO₂ clumps were as large as 4 μm . Careful inspection of the SEM indicates that the SnO₂ shows that the rock-like clumps were actually agglomerates made up of spherical nano-SnO₂ particles of a sizes less than 100 nm. Despite the effective inter-grain agglomeration between the SnO₂ nanograins, the agglomerates themselves were seen to be loosely held together within the sensor matrix, as observed in Figure 1m,n, suggesting the provision of diffusion pathways between the agglomerates [23] for the gaseous molecules to travel into and out of the body of the sensor matrix. The pure ZnO sensor sample in Figure 1a,b showed that the ZnO grains were loosely held within the matrix of the material.

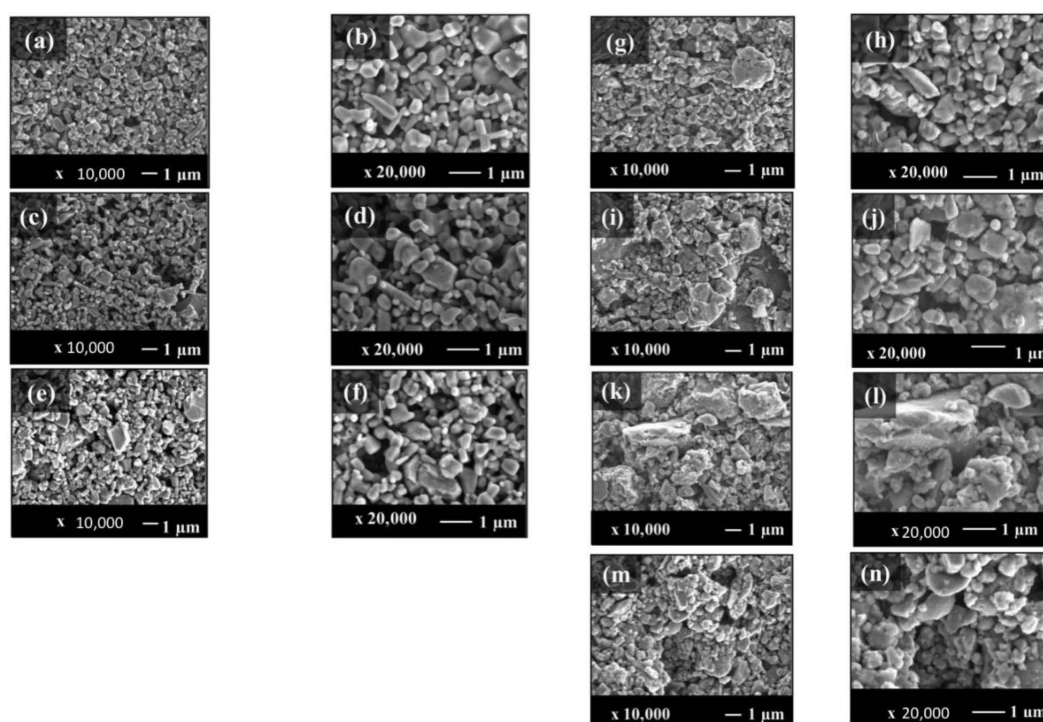


Figure 1. SEM images of (a) 100 wt% ZnO \times 10,000 magnification, (b) 100 wt% ZnO \times 20,000 magnification, (c) 90 wt% ZnO–10 wt% SnO₂ \times 10,000 magnification, (d) 90 wt% ZnO–10 wt% SnO₂ \times 20,000 magnification, (e) 70 wt% ZnO–30 wt% SnO₂ \times 10,000 magnification, (f) 70 wt% ZnO–30 wt% SnO₂ \times 20,000 magnification, (g) 50 wt% ZnO–50 wt% SnO₂ \times 10,000 magnification, (h) 50 wt% ZnO–50 wt% SnO₂ \times 20,000 magnification, (i) 30 wt% ZnO–70 wt% SnO₂ \times 10,000 magnification, (j) 30 wt% ZnO–70 wt% SnO₂ \times 20,000 magnification, (k) 10 wt% ZnO–90 wt% SnO₂ \times 10,000 magnification, (l) 10 wt% ZnO–90 wt% SnO₂ \times 20,000 magnification, (m) 100 wt% SnO₂ \times 10,000 magnification and (n) 100 wt% SnO₂ \times 20,000 magnification. All materials were screen-printed and heat-treated at 600 $^{\circ}\text{C}$ before imaging.

The stark contrast in the particle sizes of both metal oxides also suggested that within the composite, not only were hetero-junction effects introduced by the presence of grains of differing chemical natures, but also they were present due to the difference in grain size. Yamazoe *et al.* [18,21] has reported hetero-junction effects within devices incorporating grains, which were non-uniform. They had reported that the simplest factor in hetero-junction devices that contributed to the non-uniformity between the grains was the differences in grain sizes between the grains. This suggests that even in a sample that consists of particles of the same chemical nature, *i.e.*, a pure SnO₂ sample for example,

differences in the grains sizes between the SnO₂ particles can induce contact potential enhancement effects, within the matrix of the sensing material. In the case of the SnO₂–ZnO composite array examined here, multiple inhomogeneities existed to exert hetero-junction enhancement effects, which are expected to play a positive role in the overall gas-sensing properties of the materials.

As the concentrations of ZnO and SnO₂ were varied, SEM imaging showed a variation in the microstructure of the sensor devices; however, microstructures of the 90 wt% ZnO–10 wt% SnO₂ and the 10 wt. ZnO–90 wt% SnO₂ composite devices were seen to be dominated by the dominant metal oxide, *i.e.*, ZnO and SnO₂, respectively, as observed in Figure 1c,d and 1k,l, respectively, and as such, the microstructures of these composites resembled those of the corresponding pure metal oxides. This suggested homo-contact-dominated percolation paths within the sensor matrix of each composite device and a homo-contact-dominated packing structure. The 70 wt% ZnO–30 wt% SnO₂, 50 wt% ZnO–50 wt% SnO₂ and 30 wt% ZnO–70 wt% SnO₂ composite devices observed in Figure 1e,f, 1g,h and 1i,j were seen to be associated with a dispersion of both metal oxide materials, suggestive of a hetero-contact-dominated packing structure in these devices. SEM imaging did not show evidence of significant fusing between the ZnO and SnO₂ grains in the composite materials.

3.2. X-Ray Diffraction

The glancing angle XRD patterns of the devices are presented in Figure 2. The crystalline nature of both metal oxide compounds was confirmed through the observation of sharp defined peaks of both metal oxides. The XRD pattern of the SnO₂ sample confirmed that the metal oxide crystallised in a tetragonal rutile structure, matching the reference pattern (JCPDS No. 41-1445) [24–26]. The XRD pattern of ZnO showed that the metal oxide adopted a wurtzite hexagonal crystal structure (JCPDS No. 36-1451) [27–29].

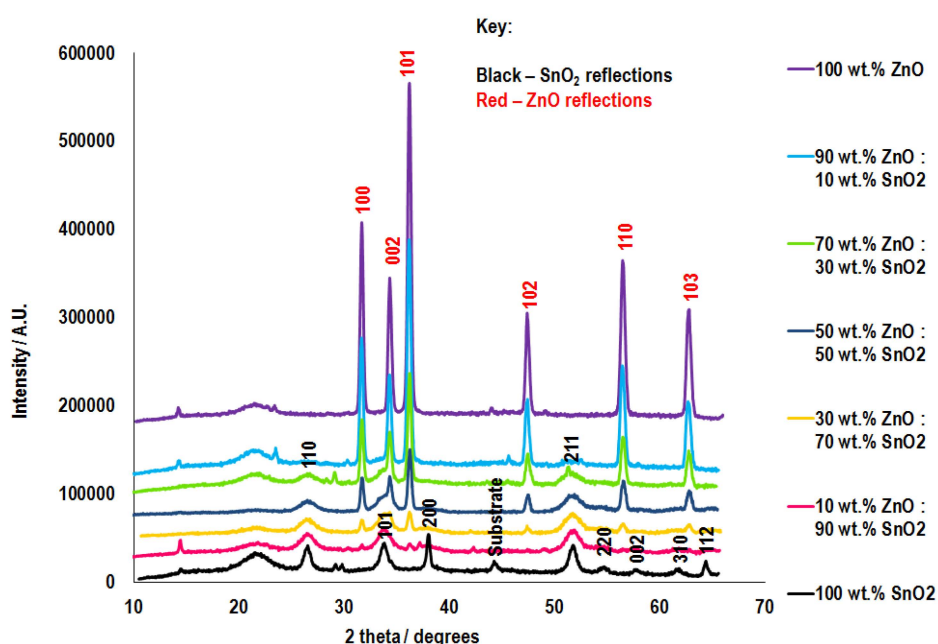


Figure 2. XRD patterns of pure and composite sensors based on SnO₂ and ZnO metal oxides, in the SnO₂–ZnO composite array. All materials were screen-printed and heat-treated at 600 °C, prior to XRD measurements.

The patterns showed the variation in the concentration of the SnO₂ and ZnO components through the gradual change in intensity of the associated peaks in the expected order. The observation of the peaks of the individual metal oxide crystal phases indicated that all materials existed in composite

form. No reflections from ternary phases were observed, although some reflections attributed to the alumina substrate were observed.

3.3. Raman Spectroscopy

Raman spectra of the sensors devices within the SnO₂-ZnO array, have been presented in Figure 3. The results corroborated the XRD showing that the Raman bands of SnO₂ matched those of a tetragonal rutile phase [26]. The three bands of SnO₂ observed in the Raman data are associated with the E_g (476 cm⁻¹), A_{1g} (633 cm⁻¹) and B_{2g} (774 cm⁻¹) vibrational modes. The Raman bands of the ZnO sample were in agreement with a wurtzite hexagonal structure [30–32].

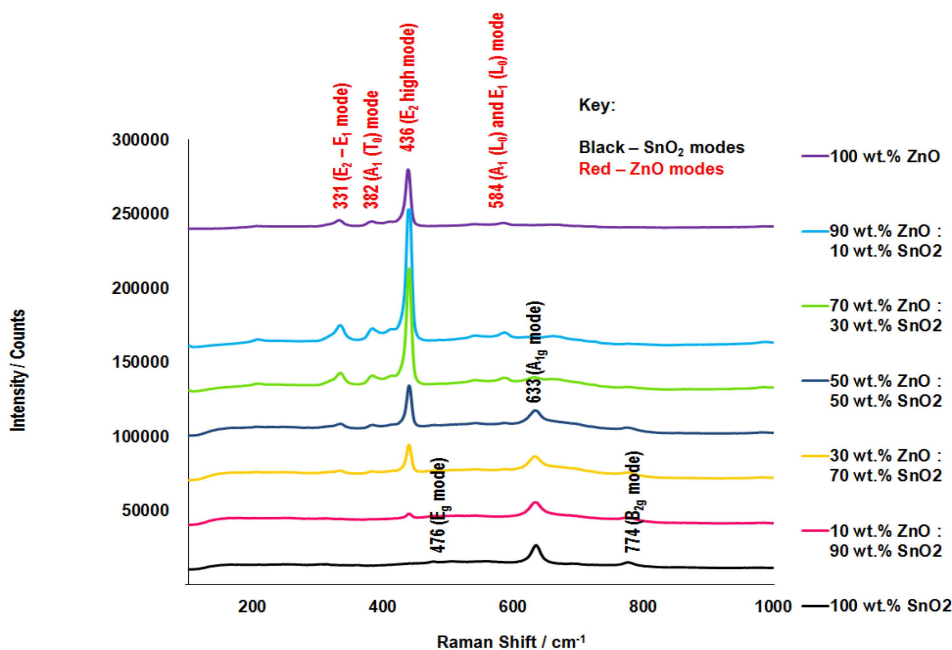


Figure 3. Raman spectra of all sensor devices within the SnO₂-ZnO sensor array. All sensors were heat-treated at 600 °C, prior to Raman spectroscopy measurements.

The Raman data showed the presence of both metal oxides within the mixed metal oxide materials, giving evidence of the composite nature of the mixtures. No peaks for any tertiary phases were observed in the Raman spectra, corroborating the XRD data, of the presence of only the two metal oxide phases in the materials.

3.4. X-Ray Photoelectron Spectroscopy

XPS measurements (Figure 4) were conducted on all sensors within the SnO₂-ZnO array, with two binding energy peaks of each metal observed for the corresponding metal oxide. All spectra (with a ±0.1 eV experimental measurement error) were standardized against the C1s binding energy of 284.6 eV obtained from the reference database [33] and from the literature [34,35]. For all ZnO-containing samples, a Zn 2p_{3/2} peak occurred in the range of 1021–1023 eV (Figure 4A), and for all SnO₂-containing samples, an Sn 3d_{5/2} peak in the range of 486–487 eV was observed (Figure 4C). All samples gave an O1s peak in the region of 531.5–532.0 eV (Figure 4B) [33]. All of the observed peaks were experimentally in agreement with the reference database [33] and accompanied by spin-orbit doublets. For the Sn species, 3d_{5/2} and 3d_{3/2} splitting values in the range of 8.4–8.7 eV were in close agreement with the literature values [36] and for Zn species, Zn2p_{3/2} and Zn2p_{1/2} splitting values in the range of 23.0–23.1 eV, which were also in close agreement with the literature values [37]. Figure 4D

shows the relative binding energies of the Zn 2p_{3/2} and Sn 3d_{5/2} peaks; the lack of significant variance in the value suggests that no significant band bending is likely to be occurring.

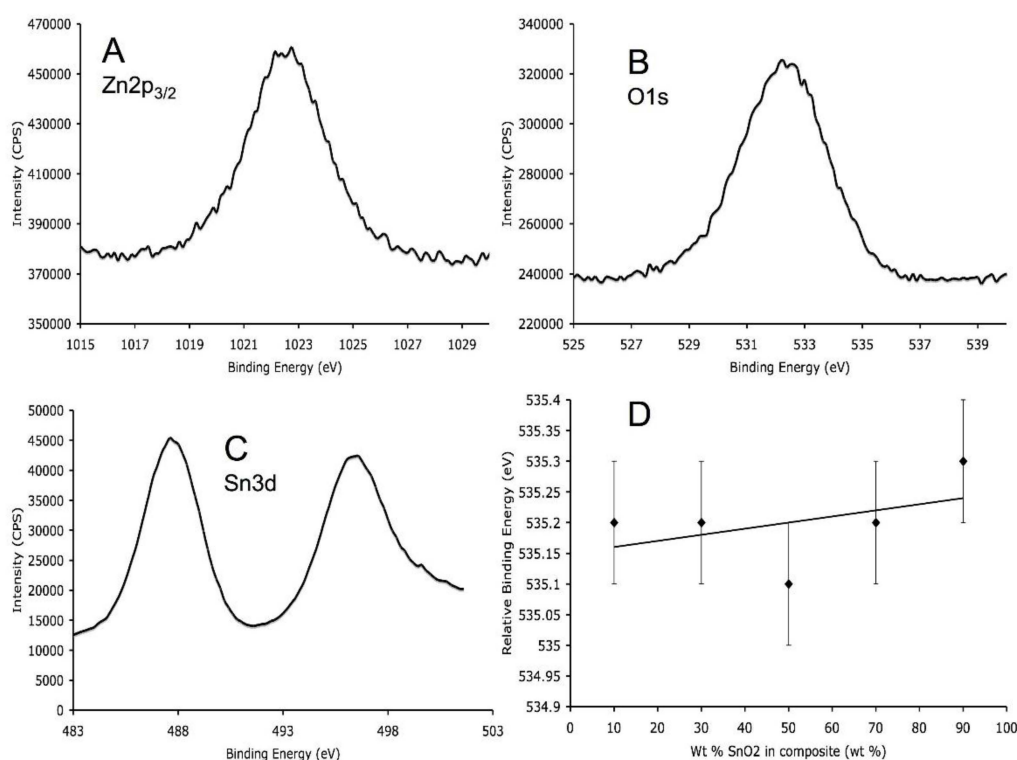


Figure 4. High resolution XPS scans of the 50 wt% ZnO:50 wt% SnO₂ sample for (A) the Zn2p_{3/2} peak, (B) the O1s peak, (C) the Sn3d peaks and (D) the XPS data of the relative binding energies (calculated by taking the difference between the B.E. of the Zn 2p_{3/2} peak and the B.E. of the Sn 3d_{5/2} peak) for all of the associated composites as a function of wt% SnO₂ in each composite.

3.5. Gas Sensing Characterisation

3.5.1. Ethanol Sensing

The conductive response traces of the array against increasing concentrations of ethanol at an operating temperature of 300 °C are presented in Figure 5. This was the temperature at which the sensors within the array exhibited the optimal response, except for the 100 wt% ZnO and 90 wt% ZnO–10 wt% SnO₂ sensor devices, both of which exhibited optimal performance at a higher temperature of 350 °C. The observed increase in conductive response of all devices against the reducing analyte is inherent to the nature of the n-type conductivity of both SnO₂ and ZnO metal oxides, whose conductive response is seen to increase upon exposure to ethanol [38]. The response behaviour therefore gave evidence that the conductivity within the pure and composite materials occurred via the n-type percolation paths that existed between the ZnO–ZnO and SnO₂–SnO₂ homo-contacts and the ZnO–SnO₂ hetero-contacts (the latter of which is only attributed to the composite materials).

The response traces in Figure 5 indicated an enhanced response of the composite devices compared to both the 100 wt% SnO₂ and 100 wt% ZnO pure counterpart devices. The highest response achieved was against 100 ppm ethanol by the 50 wt% ZnO–50 wt% SnO₂ device, which exhibited a response of 109.1, a 4.5-fold increase with respect to the pure SnO₂ counterpart (which displayed a response of 24.4) and a 12.3-fold enhancement with respect to the pure ZnO counterpart (which was associated with a response of 8.9), towards the same concentration of the analyte.

Hetero-junction enhancement effects have been postulated in the literature as a key influential factor in the enhancement effects observed in SnO₂–ZnO mixed oxide systems. Haeng Yu *et al.* [39]

for example, reported on the CO gas sensing properties of ZnO–SnO₂ composites, finding that 20–60 mol% of ZnO in SnO₂ led to an enhanced gas response towards 200 ppm of the analyte. Song *et al.* [40] also investigated the gas response towards ethanol of mesoporous ZnO–SnO₂ nanofibres and observed an increase in gas response [41].

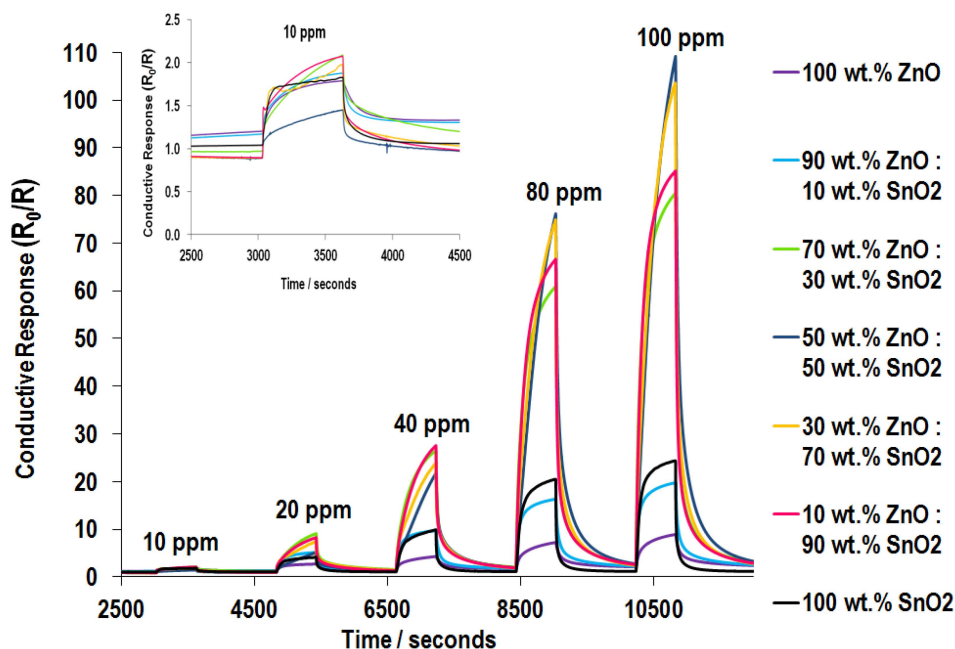


Figure 5. Conductive response traces of the SnO₂-ZnO array towards 10, 20, 40, 80 and 100 ppm ethanol gas, at an operating temperature of 300 °C. The inset zooms into the conductive response traces of the array against 10 ppm of the analyte. The best response of 110 is observed for the 50 wt% ZnO:50 wt% SnO₂ device.

The percolation pathways of devices where the homo-contacts are more dominant than the hetero-contacts are practically non-resistive. This implies that the electrons need to surmount a lower energy barrier to move through the same individual grains in the body of the material. This reasoning may aid in justifying the lower response of the 10 wt% ZnO–90 wt% SnO₂ and 70 wt% ZnO–30 wt% SnO₂ composites compared to the 50 wt% ZnO–50 wt% SnO₂ and the 30 wt% ZnO–70 wt% SnO₂ composite devices. The significant response however of both the 10 wt% ZnO–90 wt% SnO₂ and 70 wt% ZnO–30 wt% SnO₂ devices with respect to the pure SnO₂ and ZnO counterparts suggested that packing structures contained localized contact potentials that played a role in enhancing the response function of the devices.

The 90 wt% ZnO–10 wt% SnO₂ composite device was the only mixed metal oxide sensor that displayed a response behaviour that was slightly better than the ZnO counterpart, but worse than the pure SnO₂ counterpart. The device exhibited a response of 19.8 towards 100 ppm ethanol, which was a two-fold enhanced response compared to the unmodified ZnO sensor, but a 1.2-fold times poorer response compared to the unmodified SnO₂ sensor, both against 100 ppm ethanol. The composition of this particular device, as given in Table 1, showed that its matrix was dominated almost totally by the ZnO grains with very little contribution of the SnO₂ material. This suggested that the fraction of the SnO₂ grains that were present within the sea of ZnO grains was limited. As such, the percolation pathways were mainly dominated by the ZnO–ZnO homo-contacts, with hardly any percolation paths between the SnO₂-ZnO hetero-contacts, which did not influence the performance of the device with respect to the unmodified ZnO counterpart.

Apart from the hetero-junction enhancement effects associated with the SnO₂ and ZnO binary system, the synergy of the combination of both metal oxides can be postulated as playing a key role

in influencing the enhanced response behaviour observed. De Lacy Costello *et al.* [9] have reported that both SnO₂ and ZnO are well-known dehydrogenation catalysts for VOCs, such as methanol and 2-butanol and ethanol [42,43]. The group itself had reported on the catalytic and vapour-sensing properties of various SnO₂–ZnO composite devices, (1) 25 mass%:75 mass%, (2) 50 mass%:50 mass% and (3) 75 mass%:25 mass% SnO₂–ZnO, at 350 °C towards 1-butanol. They reported that composites of both metal oxides were more responsive to butanol than the pure metal oxide counterparts and had attributed this behaviour to the synergistic action of both metal oxide towards the catalytic breakdown of butanol via a dehydrogenation route (as opposed to a dehydration route). The dehydrogenation has been observed to be the more dominant pathway of the catalytic breakdown of ethanol on the surface of metal oxides [44–46]. Specifically, they had reported that the SnO₂ was very effective in the dehydrogenation of butanol to butanal and the ZnO was particularly effective not only at the dehydrogenation of the butanol to butanal, but further for the breakdown of butanal. As such, they reported that combining both metal oxides was attributed to enhanced responsivity towards the analyte, due to the independent, but synergistic catalytic breakdown mechanisms of each metal oxide of butanol. In a similar way, the catalytic dehydrogenation of ethanol may also have been influenced by the synergistic combination of both SnO₂ and ZnO metal oxides.

In comparison to the observed responses to ethanol exhibited by the SnO₂-ZnO composite system presented in this work, de Lacy Costello *et al.* [4] had reported a very similar study on SnO₂ and ZnO composite sensors for the detection of ethanol. At an operating of 350 °C, the 25 mass%:75 mass% SnO₂:ZnO sensor device was the most responsive and exhibited a maximum response of 86% change in conductivity, compared to 22% exhibited by the pure SnO₂ sensor device and 60% exhibited by the pure ZnO sensor device, all against 100 ppb ethanol. Although a direct comparison cannot be made between the literature study and that being reported here, the sensor devices reported by de Lacy Costello *et al.* [4] are seen to be very responsive, with the ability to detect ppb levels of ethanol 100-times less concentrated than the concentrations studied experimentally in this thesis. However, both studies do establish the enhancement effects achieved through a combination of SnO₂ and ZnO metal oxides. Song *et al.* [47] also reported further work on the use of ZnO–SnO₂ nanofibres prepared by electrospinning for ethanol sensing. At an operating temperature of 300 °C, against increasing concentrations of ethanol, the ratio of 2:1 Zn:Sn sol prepared nanofibres performed with a response of 10 for 50 ppm ethanol and a response of 19 towards 100 ppm ethanol.

The apparent kinetic behaviour observed from the response traces of the array in Figure 5 showed that the response of the composite materials was significantly slower than that of the pure metal oxide materials. The shark-fin behaviour of the response traces of both composites was suggestive of unsaturated sensor surfaces, with 10 minutes of ethanol exposure proving to be insufficient time to attain steady-state saturation (indeed testing with two hour-long pulses failed to induce saturated gas responses). This unsaturated behaviour was suggestive of a large number of reaction sites, with adsorbed oxygen anions readily available to react in both composite materials for the given concentration of ethanol exposure, or alternatively, too large concentrations of ethanol for the given number of reaction sites. The shark-fin behaviour was very gradual for these two best performing composites, indicating a relatively slow response behaviour. In stark contrast, the pure metal oxide materials exhibited saturated behaviour within the 10 minutes of exposure to ethanol, suggesting the presence of a limited number of reaction sites or a limited number of adsorbed oxygen anions available, for the given concentration of ethanol exposure.

An enhanced number of reaction sites in a mixed oxide system has previously been reported by Zeng *et al.* [41], who had reported on the enhanced gas-sensing properties of SnO₂ nanosphere functionalised TiO₂ nanobelts toward various VOCs. The main finding was that the nanoparticle decoration increased the number of local depleted regions. Thus, the enhanced number of the reaction sites promoted by the significant dispersion of hetero-contacts within the packing structures of both the 50 wt% ZnO–50 wt% SnO₂ and 30 wt% ZnO–70 wt% SnO₂ composites can explain the unsaturated shark-fin nature of their response traces and suggests a larger number of reaction sites available for

the given number of ethanol molecules in the exposure. As such, the reaction sites of the composite materials are unsaturated and therefore associated with slower response times. In contrast, a limited number of reaction sites in the pure metal oxide materials suggests faster saturation of the surfaces, accounting for the faster response times.

The shark-fin behaviour for the 10 wt% ZnO–90 wt% SnO₂ and 70 wt% ZnO–30 wt% SnO₂ composites was less pronounced (Figure 5). This faster behaviour of both of these composites suggested a reduced number of reaction sites of interaction for the given number of ethanol molecules that they were exposed to, justified by the homo-contact-dominated packing-structures of both composites.

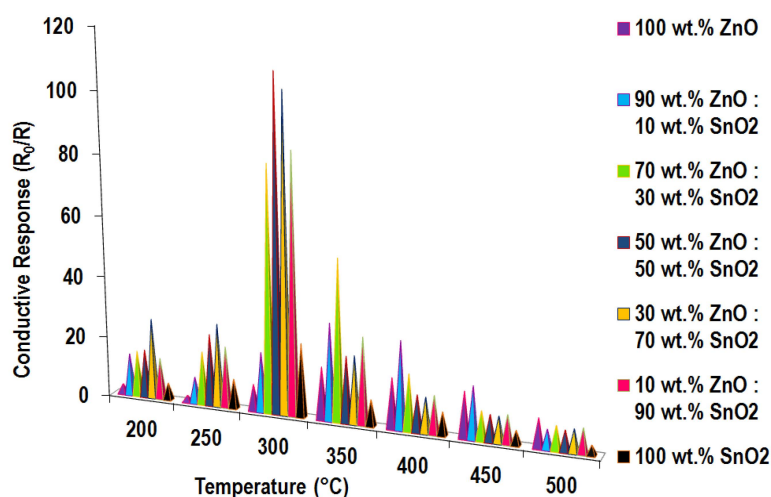


Figure 6. Conductive response of the SnO₂-ZnO array against 100 ppm ethanol gas, as a function of increasing operating temperature. The best response of 110 is observed for the 50 wt% ZnO:50 wt% SnO₂ device at an operating temperature of 300 °C.

Figure 6 presents the conductive response of the array of sensors towards 100 ppm ethanol as a function of increasing operating temperature. The figure illustrates that 300 °C was the optimal operating temperature for almost all sensor devices within the array, with the 90 wt% ZnO–10 wt% SnO₂ and pure ZnO sensor devices performing optimally at a higher operating temperature of 350 °C. The operating temperature of 300 °C was the optimal temperature of operation for the array of sensor devices, with a large distribution of response magnitudes exhibited by the array of sensor devices against the range of concentrations of ethanol exposure.

As observed in Figure 6, at the lower operating temperature of 200 °C, the hetero-junction enhancement effects were still visible with enhanced response of the composite materials with respect to the pure counterparts, albeit at a lower response magnitude. The conductive response of the array of sensors at the highest operating temperature of 500 °C seen in Figure 7 showed that responses of all sensor devices significantly decreased in the comparison at the response magnitudes observed at the lower operating temperatures of 200 °C and 300 °C.

3.5.2. NO₂ Sensing

Figure 7 illustrates the resistive response traces of the array of sensors against increasing concentrations of NO₂ at the optimal operating temperature of 300 °C. The figure indicates that the resistive response order of the array of devices increased as a function of increasing ZnO concentration or as a function of decreasing concentration of SnO₂, when exposed to 800 ppb NO₂. At this highest concentration of NO₂ exposure, the results show that the array did not exhibit hetero-junction or synergistic enhancement effects when exposed to the oxidising gas, in stark contrast to what was observed for ethanol. Towards 800 ppb, the pure ZnO sensor device exhibited the strongest resistive response (of all sensor devices) of 121.6, and the pure SnO₂ sensor in contrast exhibited the weakest

resistive response (of all sensors devices) of 10.7. Figure 7 shows that as the concentration of NO_2 was increased from 200 ppb to 800 ppb, an exponential increase in the response of the ZnO sensor device was observed, which suggested the lack of saturation of the surface sites, accounted for by the low concentration (ppb) regime of NO_2 exposure and that higher concentrations of exposure were therefore required for the sensor surface to saturate.

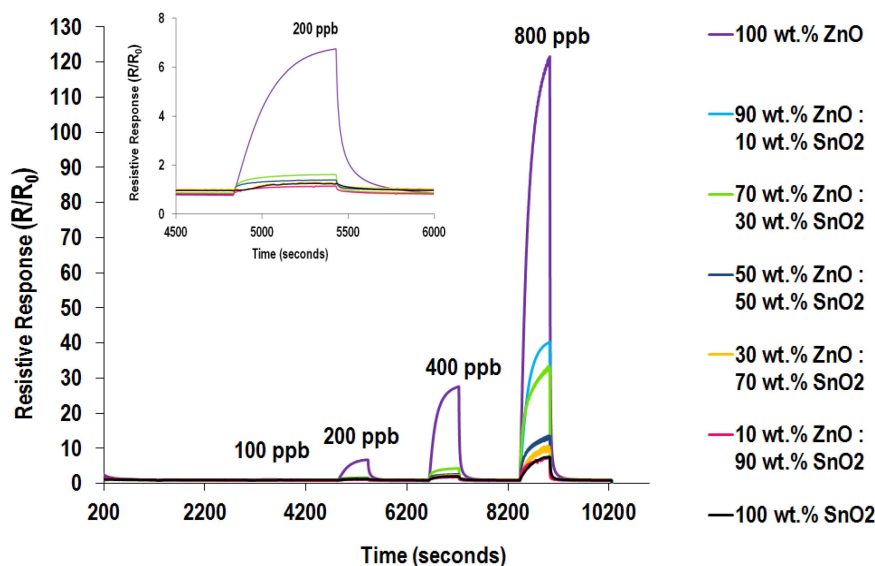


Figure 7. Resistive response traces of SnO_2 -ZnO array towards 100, 200, 400 and 800 ppb NO_2 gas, at an operating temperature of 300 °C. The inset projects the resistive responses of the array towards 200 ppb NO_2 . The best response of 120 is observed for the 100 wt% ZnO device.

Figure 8 presents the resistive response of the array of sensors towards 800 ppb NO_2 , as a function of increasing operating temperature. The figure established that the pure ZnO sensor dominated the response at all operating temperatures and that the response magnitudes of the rest of the array decreased as a function of decreasing concentration of ZnO at all operational temperatures. Further, the figure illustrates that the response of the sensor devices decreases as a function of increasing operating temperature with the optimal response of the sensors at 300 °C.

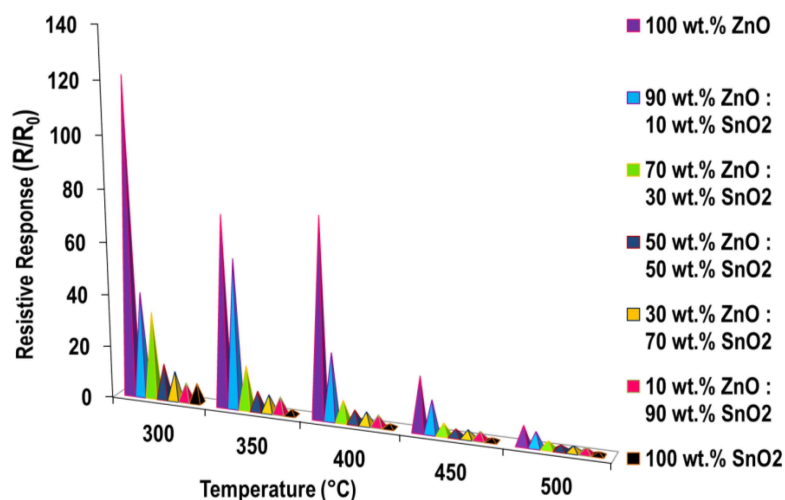


Figure 8. Resistive responses of the SnO_2 -ZnO array towards 800 ppb NO_2 gas as a function of increasing operating temperature. The best response of 120 is observed for the 100 wt% ZnO device at an operating temperature of 300 °C.

Park *et al.* [48] reported a hybrid SnO₂-ZnO electrospun nanofibre that is highly sensitive towards NO₂. The sensor gave the highest resistive response of 100 at an operating temperature of 180 °C. Song *et al.* [47] also report that their nanofibre sensor prepared with a molar ratio of the precursor sols of Zn:Sn of 2:1 only showed a response of one towards 100 ppm NO₂. In Song *et al.*'s work, the structure was of a true composite comparable to our work here, as opposed to Park *et al.*, who report a core-shell type structure [48]. This suggests that the packing structure of the metal oxides with respect to each other can significantly influence the responsivity and selectivity towards particular analytes and that those packing structures containing composites of both SnO₂ and ZnO are better suited for VOC detection.

Xu *et al.* [49] reported the NO₂ gas sensing properties of SnO₂-ZnO porous nano-solids produced via a solvothermal hot-press (SHP) method. When exposed to 35 ppm NO₂, the composites were seen to exhibit enhanced responses compared to the pure SnO₂ porous nanosolid counterpart. The best response of 75 was observed at an operating temperature of 225 °C by a composite sensor containing SnO₂ loaded with 20 wt% ZnO. In contrast to the SnO₂-ZnO composites reported in this work and in the literature by Song *et al.* [47], the composites prepared by Xu *et al.* [49] did exhibit a significant gas responses towards NO₂, although at a much higher concentration than investigated here.

3.5.3. Cross Sensitivity Testing

A cross-sensitivity analysis of the SnO₂-ZnO array was conducted towards a range of reducing gases, acetone, CO and NH₃, at an operating temperature of 300 °C. This was the temperature at which most sensors in the array performed optimally against the key reducing gas, ethanol, as seen in Figure 5.

NH₃ Sensing

The response results of the array against 20 ppm NH₃, which was the largest concentration the array was exposed to, are presented in Figure 9. Most of the sensors in the array were attributed to responses close to the baseline response of one, with only the pure SnO₂ showing a response of two. Interestingly, the SnO₂, 90 wt% SnO₂-10 wt% ZnO and 70 wt% SnO₂-30 wt% ZnO sensor devices were seen to be attributed to conventional n-type response characteristics against the analyte; however, all other n-type devices, which had a significant contribution of ZnO, were attributed to unconventional p-type response behaviour. Such resistive response of n-type materials against NH₃ has been observed previously in the literature due to the NH₃ undergoing oxidation reactions on the surface of metal oxides [50,51]. The reaction process can follow one of many routes, allowing several possible competing processes to all take place at the same time. One of the reactions leads to the combustion of NH₃ to NO, which is easily converted to NO₂ in the presence of oxygen. NO₂ is an oxidising gas, and therefore, the materials are likely to exhibit an increase in resistive response, upon contact with the n-type semiconducting oxides.

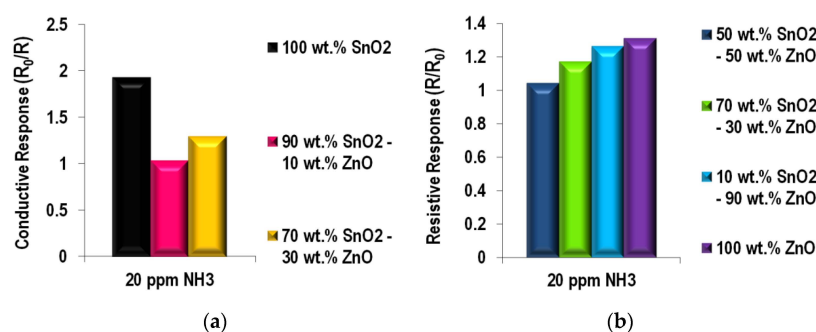


Figure 9. (a) Conductive responses and (b) resistive responses of the SnO₂-ZnO array against 20 ppm NH₃ at an operating temperature of 300 °C.

Acetone Sensing

Figure 10 presents the conductive responses of the array of sensor devices against increasing concentrations of acetone gas at an operating temperature of 300 °C. The graph shows that the sensors were responsive to a concentration as low as 1 ppm acetone. As the concentration of acetone exposure was increased, the graphs show that the response of the array randomises in terms of response order, with the composite materials exhibiting significantly enhanced responses compared to the pure counterparts. The 70 wt% ZnO–30 wt% SnO₂ sensor was the best performing composite sensor device of the array, with the best response of 32.9 towards 10 ppm of the analyte. This was a 5.5-fold enhanced response with respect to the pure SnO₂ counterpart (which exhibited a response of 6.4) and a 3.3-fold enhanced response compared the pure ZnO counterpart (which exhibited a response of 9.8) at the same analyte concentration of 10 ppm. The particularly enhanced response of this composite, against the poor response of both the individual metal oxides, is suggestive of synergistic and hetero-junction effects playing a role to enhance the response characteristics. A comparison of Figure 11 with respect to an exposure of 10 ppm of ethanol at the same operating temperature, observed in Figure 5, shows the array of SnO₂-ZnO sensor devices were more selective towards 10 ppm acetone. The highest response observed against 10 ppm ethanol was 2.1 by the 10 wt% ZnO–90 wt% SnO₂ sensor device. Thus, of the two VOCs, the array can be established as being selective towards acetone. In particular, the conductive response of the 70 wt% ZnO–30 wt% SnO₂ composite is seen to increase exponentially as a function of increasing acetone concentration, which suggests that the surface of the composite remains unsaturated upon each exposure concentration introduced. In contrast, the conductive response magnitudes of the pure metal oxides, in particular the SnO₂ material, are seen to increase gradually and slowly as a function of increasing acetone concentration, which indicates the saturation of the surfaces as a function of the increased concentration. A similar behaviour of the devices was observed as a function of increasing ethanol concentration and can be accounted for by the increased number of reaction sites in the composite materials, due to the presence of the hetero-contacts in the composite materials.

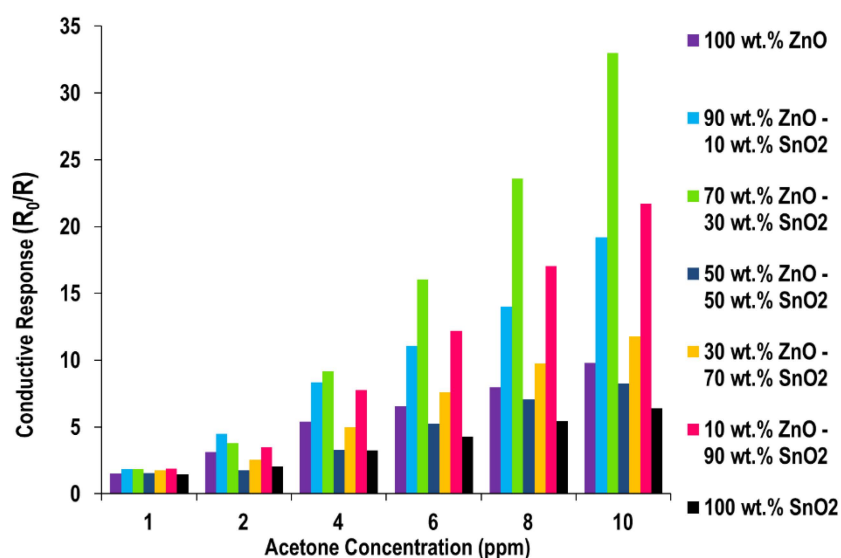


Figure 10. Conductive responses of SnO₂-ZnO array towards 1, 2, 4, 6, 8 and 10 ppm acetone gas, at an operating temperature of 300 °C. The best response of 34 is observed for the 70 wt% ZnO:30 wt% SnO₂ device on exposure to 10 ppm of acetone.

CO Sensing

Figure 11 presents the conductive responses of the array of SnO₂-ZnO sensor devices against increasing concentrations of CO at an operating temperature of 300 °C. The graph illustrates that the

pure SnO₂ sensor was associated with the most effective response behaviour of all sensor devices with a maximum response of 5.7 observed against 1000 ppm CO. The pure ZnO sensor in contrast was associated with a response of 1.6 towards the same concentration of CO. In general, the response graph shows that the response of the sensors increased as a function of increasing concentration of SnO₂ and decreasing concentration of ZnO, which is analogous to the behaviour observed against NO₂; however, for the oxidising gas, the trend was observed to be an increase in resistive response as a function of increasing concentration of ZnO and decreasing concentration of SnO₂. Thus, the response trend observed against CO was observed to be dominated by the presence of SnO₂.

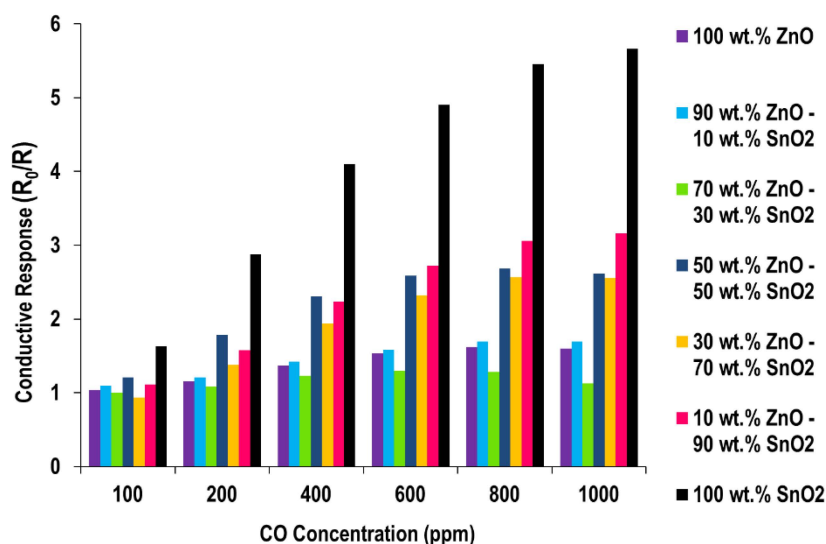


Figure 11. Conductive responses of SnO₂-ZnO array towards 100, 200, 400, 600, 800 and 1000 ppm CO gas, at an operating temperature of 300 °C. The best response of 5.9 is observed for the 100 wt% SnO₂ device towards 1000 ppm of CO.

With respect to ethanol and acetone response, Figure 11 confirms that the responses towards CO were poor and that the selectivity of the array is towards acetone. Further, a difference in the enhancement contributor was visible between all three reducing analytes, with greater synergistic catalysis and hetero-junction enhancement effects contributing to the extensive response of the composite materials towards both ethanol and acetone and, in contrast, dominance of the SnO₂ metal oxide concentration contributing towards the responses observed against CO.

4. Conclusions

Results and analysis from this study showed that the array of SnO₂-ZnO composite sensors were most effective for the detection of both ethanol and acetone. In particular, the composites materials were seen to exhibit significantly better response behaviours than the pure counterparts towards both analytes. The best performing composite towards ethanol was seen to be the 50 wt% ZnO-50 wt% SnO₂ sensor device at 300 °C with a response of 109 towards 100 ppm of the analyte. The 70 wt% ZnO-30 wt% SnO₂ sensor device was the prime candidate for acetone sensing, with the largest observed response of 33 towards 10 ppm of the analyte at 300 °C. The comparison of the response behaviour of the SnO₂-ZnO array towards 10 ppm acetone and 10 ppm ethanol indicated that if the array were put in a mixed atmosphere of 10 ppm of both analytes, it could potentially discriminate between ethanol and acetone and exhibit selectivity towards acetone. These results thus showed that a simple change in the concentration of the individual metal oxides within the composites could tune the gas response and selectivity of the devices towards a particular analyte. The response behaviour towards both NO₂ and CO was relatively poor, suggesting that operating in an environment where these gases were present would not cause a significant concern regarding cross sensitivity.

Our analysis suggests that the synergistic enhancement effects of both metal oxides weigh out the hetero-junction enhancement effects, and therefore, the extensive gas response of the hetero-junction system is likely due to the synergy of the combination of metal oxide components. The hetero-junction enhancement effects are thought to play a supporting role to influence the better performance of the composite materials. Further, the study has demonstrated that a simple change in the concentration of SnO₂ and ZnO in composite form and random packing structures of SnO₂ and ZnO grains in composite matrices are an effective way to achieve stark enhancements in the response behaviour.

Acknowledgments: Kevin Reeves, Martin Vickers, Steve Firth and Robert Palgrave are thanked for help with the analysis.

Conflicts of Interest: The authors declare no conflict of interest.

References

1. Capone, S.; Forleo, A.; Francioso, L.; Rella, R.; Siciliano, P.; Spadavecchia, J.; Presicce, D.S.; Taurino, A.M. Solid state gas sensors: State of the art and future activities. *J. Optoelectron. Adv. Mater.* **2003**, *5*, 1335–1348. [[CrossRef](#)]
2. Wang, C.X.; Yin, L.W.; Zhang, L.Y.; Xiang, D.; Gao, R. Metal Oxide Gas Sensors: Sensitivity and Influencing Factors. *Sensors* **2010**, *10*, 2088–2106. [[CrossRef](#)] [[PubMed](#)]
3. Trakhtenberg, L.I.; Gerasimov, G.N.; Gromov, V.F.; Brelysheva, T.V.; Ilegbusi, O.J. Gas Semiconducting Sensors Based on Metal Oxide Nanocomposites. *J. Mater. Sci. Res.* **2012**, *1*, 56–68. [[CrossRef](#)]
4. Costello, B.P.J.d.; Ewen, R.J.; Guernion, N.; Ratcliffe, N.M. Highly sensitive mixed oxide sensors for the detection of ethanol. *Sens. Actuators B: Chem.* **2002**, *87*, 207–210. [[CrossRef](#)]
5. Tang, H.; Yan, M.; Zhang, H.; Li, S.; Ma, X.; Wang, M.; Yang, D. A selective NH₃ gas sensor based on Fe₂O₃–ZnO nanocomposites at room temperature. *Sens. Actuators B: Chem.* **2006**, *114*, 910–915. [[CrossRef](#)]
6. Bai, S.; Li, D.; Han, D.; Luo, R.; Chen, A.; Chung, C.L. Preparation, characterization of WO₃–SnO₂ nanocomposites and their sensing properties for NO₂. *Sens. Actuators B: Chem.* **2010**, *150*, 749–755. [[CrossRef](#)]
7. Ivanovskaya, M.; Kotsikau, D.; Faglia, G.; Nelli, P. Influence of chemical composition and structural factors of Fe₂O₃/In₂O₃ sensors on their selectivity and sensitivity to ethanol. *Sens. Actuators B: Chem.* **2003**, *96*, 498–503. [[CrossRef](#)]
8. Sun, C.; Maduraiveeran, G.; Dutta, P. Nitric oxide sensors using combination of p- and n-type semiconducting oxides and its application for detecting NO in human breath. *Sens. Actuators B: Chem.* **2013**, *186*, 117–125. [[CrossRef](#)]
9. Costello, B.P.J.d.; Ewen, R.J.; Jones, P.R.H.; Ratcliffe, N.M.; Wat, R.K.M. A study of the catalytic and vapour-sensing properties of zinc oxide and tin dioxide in relation to 1-butanol and dimethyldisulphide. *Sens. Actuators B: Chem.* **1999**, *61*, 199–207. [[CrossRef](#)]
10. Kaciulis, S.; Pandolfi, L.; Viticoli, S.; Sberveglieri, G.; Zampiceni, E.; Wlodarski, W.; Galatsis, K.; Li, Y.X. Investigation of thin films of mixed oxides for gas-sensing applications. *Surf. Interface Anal.* **2002**, *34*, 672–676. [[CrossRef](#)]
11. Barreca, D.; Carraro, G.; Comini, E.; Gasparotto, A.; Maccato, C.; Sada, C.; Sberveglieri, G.; Tondello, E. Novel Synthesis and Gas Sensing Performances of CuO–TiO₂ Nanocomposites Functionalized with Au Nanoparticles. *J. Phys. Chem. C* **2011**, *115*, 10510–10517. [[CrossRef](#)]
12. Zakrzewska, K. Mixed oxides as gas sensors. *Thin Solid Films* **2001**, *391*, 229–238. [[CrossRef](#)]
13. Yamazoe, N.; Tamaki, J.; Miura, N. Role of hetero-junctions in oxide semiconductor gas sensors. *Mater. Sci. Eng. B* **1996**, *41*, 178–181. [[CrossRef](#)]
14. Costello, B.P.D.; Ewen, R.J.; Ratcliffe, N.M.; Sivanand, P. Thick film organic vapour sensors based on binary mixtures of metal oxides. *Sens. Actuators B: Chem.* **2003**, *92*, 159–166. [[CrossRef](#)]
15. Chen, Y.; Xiao, G.; Wang, T.; Zhang, F.; Ma, Y.; Gao, P.; Zhu, C.; Zhang, E.; Xu, Z.; Li, Q. Synthesis and enhanced gas sensing properties of crystalline CeO₂/TiO₂ core/shell nanorods. *Sens. Actuators B: Chem.* **2011**, *156*, 867–874. [[CrossRef](#)]
16. Eranna, G.; Joshi, B.C.; Runthala, D.P.; Gupta, R.P. Oxide materials for development of integrated gas sensors—A comprehensive review. *Crit. Rev. Solid State Mater. Sci.* **2004**, *29*, 111–188. [[CrossRef](#)]

17. Wager, J.F. Transparent electronics: Schottky barrier and heterojunction considerations. *Thin Solid Films* **2008**, *516*, 1755–1764. [[CrossRef](#)]
18. Yamazoe, N.; Shimano, K. Proposal of contact potential promoted oxide semiconductor gas sensor. *Sens. Actuators B: Chem.* **2013**, *187*, 162–167. [[CrossRef](#)]
19. Jayalakshmi, M.; Balasubramanian, K. Hydrothermal Synthesis of CuO-SnO₂ and CuO-SnO₂-Fe₂O₃ Mixed Oxides and Electrochemical Characterization in Neutral Electrolyte. *Int. J. Electrochem. Sci.* **2009**, *4*, 571–581.
20. Zeng, W.; Liu, T.; Wang, Z. Enhanced gas sensing properties by SnO₂ nanosphere functionalized TiO₂ nanobelts. *J. Mater. Chem.* **2012**, *22*, 3544–3548. [[CrossRef](#)]
21. Yamazoe, N.; Shimano, K. Basic approach to the transducer function of oxide semiconductor gas sensors. *Sens. Actuators B: Chem.* **2011**, *160*, 1352–1362. [[CrossRef](#)]
22. Binions, R.; Afonja, O.A.; Dungey, S.; Lewis, D.W.; Parkin, I.P.; Williams, D.E. Discrimination Effects in Metal Oxide Semiconductor Gas Sensors. *IEEE Sens. J.* **2011**, *11*, 1145–1151. [[CrossRef](#)]
23. Korotcenkov, G. The role of morphology and crystallographic structure of metal oxides in response of conductometric-type gas sensors. *Mater. Sci. Eng. R.* **2008**, *61*, 1–39. [[CrossRef](#)]
24. Liu, X.; Zhang, J.; Guo, X.; Wu, S.; Wang, S. Enhanced sensor response of Ni-doped SnO₂ hollow spheres. *Sens. Actuators B: Chem.* **2011**, *152*, 162–167. [[CrossRef](#)]
25. Lupan, O.; Chow, L.; Chai, G.; Schulte, A.; Park, S.; Heinrich, H. A rapid hydrothermal synthesis of rutile SnO₂ nanowires. *Mater. Sci. Eng. B* **2009**, *157*, 101–104. [[CrossRef](#)]
26. Sun, S.H.; Meng, G.W.; Zhang, G.X.; Gao, T.; Geng, B.Y.; Zhang, L.D.; Zuo, J. Raman scattering study of rutile SnO₂ nanobelts synthesized by thermal evaporation of Sn powders. *Chem. Phys. Lett.* **2003**, *376*, 103–107. [[CrossRef](#)]
27. Sin, N.D.M.; Kamel, M.F.; Alip, R.I.; Mohamad, Z.; Rusop, M. The Electrical Characteristics of Aluminium Doped Zinc Oxide Thin Film for Humidity Sensor Applications. *Adv. Mater. Sci. Eng.* **2011**, *2011*, 1–5. [[CrossRef](#)]
28. Anderson, J.; Chris, G.V.d.W. Fundamentals of zinc oxide as a semiconductor. *Rep. Prog. Phys.* **2009**, *72*, 126501.
29. Zhang, Y.; Zhu, F.; Zhang, J.; Xia, L. Converting Layered Zinc Acetate Nanobelts to One-dimensional Structured ZnO Nanoparticle Aggregates and their Photocatalytic Activity. *Nanoscale Res. Lett.* **2008**, *3*, 201–204. [[CrossRef](#)]
30. Huang, Y.; Liu, M.; Li, Z.; Zeng, Y.; Liu, S. Raman spectroscopy study of ZnO-based ceramic films fabricated by novel sol-gel process. *Mater. Sci. Eng., B* **2003**, *97*, 111–116. [[CrossRef](#)]
31. Loudon, R. The Raman effect in crystals. *Adv. Phys.* **2001**, *50*, 813–864. [[CrossRef](#)]
32. Choopun, S.; Hongsith, N.; Mangkorntong, P.; Mangkorntong, N. Zinc oxide nanobelts by RF sputtering for ethanol sensor. *Phys. E: Low-dimensional Syst. Nanostruct.* **2007**, *39*, 53–56. [[CrossRef](#)]
33. LaSurface.com. *Database*, Available from: <http://www.lasurface.com/database/elementxps.php>. (accessed on 10 November 2015).
34. Dementjev, A.P.; de Graaf, A.; van de Sanden, M.C.M.; Maslakov, K.I.; Naumkin, A.V.; Serov, A.A. X-Ray photoelectron spectroscopy reference data for identification of the C₃N₄ phase in carbon–nitrogen films. *Diamond Relat. Mater.* **2000**, *9*, 1904–1907. [[CrossRef](#)]
35. Boyd, K.J.; Marton, D.; Todorov, S.S.; Al-Bayati, A.H.; Kulik, J.; Zuhr, R.A.; Rabalais, J.W. Formation of C–N thin films by ion beam deposition. *J. Vac. Sci. Technol. A* **1995**, *13*, 2110–2122. [[CrossRef](#)]
36. Akgul, F.A.; Gumus, C.; Er, A.O.; Farha, A.H.; Akgul, G.; Ufuktepe, Y.; Liu, Z. Structural and electronic properties of SnO₂. *J. Alloys Compd.* **2013**, *579*, 50–56. [[CrossRef](#)]
37. Biesinger, M.C.; Lau, L.W.M.; Gerson, A.R.; Smart, R.S.C. Resolving surface chemical states in XPS analysis of first row transition metals, oxides and hydroxides: Sc, Ti, V, Cu and Zn. *Appl. Surf. Sci.* **2010**, *257*, 887–898. [[CrossRef](#)]
38. Kim, K.; Cho, P.; Kim, S.; Lee, J.; Kang, C.; Kim, J.; Yoon, S. The selective detection of C₂H₅OH using SnO₂–ZnO thin film gas sensors prepared by combinatorial solution deposition. *Sens. Actuators B: Chem.* **2007**, *123*, 318–324. [[CrossRef](#)]
39. Yu, J.H.; Choi, G.M. Electrical and CO gas sensing properties of ZnO–SnO₂ composites. *Sens. Actuators B: Chem.* **1998**, *52*, 251–256.
40. Song, X.; Wang, Z.; Liu, Y.; Wang, C.; Li, L. A highly sensitive ethanol sensor based on mesoporous ZnO–SnO₂ nanofibers. *Nanotechnology* **2009**, *20*, 075501. [[CrossRef](#)] [[PubMed](#)]

41. Zeng, W.; Liu, T.; Wang, Z. Enhanced gas sensing properties by SnO₂ nanosphere functionalized TiO₂ nanobelts. *J. Mater. Chem.* **2012**, *22*, 3544–3548. [[CrossRef](#)]
42. Halawy, S.A.; Mohamed, M.A. The effect of different ZnO precursors on the catalytic decomposition of ethanol. *J. Mol. Catal. A: Chem.* **1995**, *98*, L63–L68. [[CrossRef](#)]
43. Cheong, H.; Lee, M. Sensing characteristics and surface reaction mechanism of alcohol sensors based on doped SnO₂. *J. Ceram. Process. Res.* **2006**, *7*, 183–191.
44. Xu, J.; Han, J.; Zhang, Y.; Sun, Y.a.; Xie, B. Studies on alcohol sensing mechanism of ZnO based gas sensors. *Sens. Actuators B: Chem.* **2008**, *132*, 334–339. [[CrossRef](#)]
45. Tricoli, A.; Righettoni, M.; Teleki, A. Semiconductor Gas Sensors: Dry Synthesis and Application. *Angew. Chem. Int. Ed.* **2010**, *49*, 7632–7659. [[CrossRef](#)] [[PubMed](#)]
46. Khadayate, R.S.; Waghulde, R.B.; Wankhede, M.G.; Sali, J.V.; Patil, P.P. Ethanol vapour sensing properties of screen printed WO₃ thick films. *Bull. Mater. Sci.* **2007**, *30*, 129–133. [[CrossRef](#)]
47. Song, X.; Liu, L. Characterization of electrospun ZnO–SnO₂ nanofibers for ethanol sensor. *Sens. Actuators A* **2009**, *154*, 175–179. [[CrossRef](#)]
48. Park, J.; Moon, J.; Lee, S.; Kim, S.H.; Chu, H.Y.; Zyung, T. SnO₂–ZnO hybrid nanofibers-based highly sensitive nitrogen dioxides sensor. *Sens. Actuators B: Chem.* **2010**, *145*, 592–595. [[CrossRef](#)]
49. Xu, H.; Chen, X.; Zhang, J.; Wang, J.; Cao, B.; Cui, D. NO₂ gas sensing with SnO₂–ZnO/PANI composite thick film fabricated from porous nanosolid. *Sens. Actuators B: Chem.* **2013**, *176*, 166–173. [[CrossRef](#)]
50. Jiménez, I.; Vila, A.M.; Calveras, A.C.; Morante, J.R. Gas-sensing properties of catalytically modified WO₃ with copper and vanadium for NH₃ detection. *IEEE Sens. J.* **2005**, *5*, 385–391. [[CrossRef](#)]
51. Jiménez, I.; Centeno, M.A.; Scotti, R.; Morazzoni, F.; Cornet, A.; Morante, J.R. NH₃ Interaction with Catalytically Modified Nano-WO₃ Powders for Gas Sensing Applications. *J. Electrochem. Soc.* **2003**, *150*. [[CrossRef](#)]



© 2016 by the authors; licensee MDPI, Basel, Switzerland. This article is an open access article distributed under the terms and conditions of the Creative Commons by Attribution (CC-BY) license (<http://creativecommons.org/licenses/by/4.0/>).